DALTON

Structural and solution studies of diiodine charge-transfer complexes of thioether crowns

Alexander J. Blake,[a,b] Franco Cristiani,[c] Francesco A. Devillanova,*[,c] Alessandra Garau,[c] Liam M. Gilby,[b] Robert O. Gould,[b] Francesco Isaia,[c] Vito Lippolis,[a,c] Simon Parsons,[b] Christian Radek[b] and Martin Schröder*[,a,b]

[a] *Department of Chemistry, The University of Nottingham, University Park, Nottingham NG7 2RD, UK*
[b] *Department of Chemistrty, The University of Edinburgh, West Mains Road, Edinburgh EH9 3JJ, UK*
[c] *Dipartmento di Chimica e Tecnologie Inorganiche e Metallorganiche, University of Cagliari, Via Ospedale 72, 09124 Cagliari, Italy*

The charge-transfer complexes 2[9]aneS_3·4I_2 ([9]aneS_3 = 1,4,7-trithiacyclononane), [12]aneS_4·I_2 ([12]aneS_4 = 1,4,7,10-tetrathiacyclododecane), [14]aneS_4·I_2, [14]aneS_4·2I_2 ([14]aneS_4 = 1,4,8,11-tetrathiacyclotetradecane), [16]aneS_4·I_2 and [16]aneS_4·4I_2 ([16]aneS_4 = 1,5,9,13-tetrathiacyclohexadecane) have been prepared by slow evaporation of solutions containing I_2 and the appropriate thioether macrocycle in CH_2Cl_2. The structure of 2[9]aneS_3·4I_2 shows two independent macrocycles in the asymmetric unit which are linked by a diiodine bridge. Asymmetric units are linked by I · · · I and S · · · I interactions to form an extended array of linked macrocycles. The single-crystal structure of [12]aneS_4·I_2 features an infinite chain structure formed by alternating [12]aneS_4 and I_2 molecules. The structure contains both symmetric and asymmetric diiodine bridges. Although the 1:1 adduct [14]aneS_4·I_2 can also be described as a one-dimensional infinite chain structure with asymmetric diiodine bridging, the structure is better visualised as alternating layers of macrocycle and iodine spanned by short contacts of 3.335(4) Å. The adduct [14]aneS_4·2I_2 shows two independent macrocycles each co-ordinated to two I_2 molecules. The charge-transfer network consists of chains of molecules with alternating orientations. The single-crystal structure of a third 1:1 adduct [16]aneS_4·I_2 contains only symmetrical diiodine bridges between neighbouring macrocycles leading to an infinite chain structure. The compound [16]aneS_4·4I_2 is the first example of a tetradentate macrocycle which incorporates I_2 bound to all four S atoms. The single-crystal structure shows four terminal I_2 molecules co-ordinated to the four S donors of the macrocycle. Molecules are linked into interwoven sheets by I · · · I interactions of 3.639(2) Å. The formation enthalpies (ΔH) and constants (K) of 1:1 adducts obtained by treating various thioether macrocycles with I_2 in CH_2Cl_2 have been determined by electronic spectroscopy. The Fourier-transform Raman spectra for all the charge-transfer adducts have been recorded in CH_2Cl_2 solutions at different concentrations. The Raman frequencies of the ν(I–I) vibrations show good correlation with the measured formation enthalpies ΔH.

Many examples of charge-transfer complexes between halogens and interhalogens, particularly ICl, Br_2 and I_2, and donors such as amines,[1] phosphines,[2] ethers,[3] thioketones,[4,5] thioethers,[6–11] selenoketones[5] and selenoethers[12] have been reported. Donation of electron density from non-bonding orbitals of the donor atom into the LUMO (lowest unoccupied molecular orbital) of the dihalogen molecule, which is an antibonding σ_u* orbital lying along the main axis of the dihalogen, decreases the bond order thus increasing the bond lengths in the halogen molecule. Solid I_2 forms a layered structure where iodine molecules form a distorted honeycomb structure in each layer. The I–I bond length [2.715(6) Å][13] is elongated compared to that in the gas phase [2.667(2) Å][14] and this deviation can be attributed directly to donation of electron density from filled non-bonding p orbitals to the antibonding LUMO of a neighbouring I_2 molecule. The elongation of the I–I bond and the angle between the I_2 molecule and the donor atom, which should be approximately linear, can therefore be used as a sensitive probe in the investigation of co-ordinative bonding in solution and the solid state.

The electronic features of donor–acceptor complexes containing I_2 are in general well established, although few adducts between I_2 and small organic molecules containing more than one donor atom have been investigated. We argued that adducts of I_2 with polydentate organic molecules should be capable of forming a number of structurally diverse assemblies in the solid state. We report herein a study on charge-transfer adducts of homoleptic thioether macrocycles with varying I_2 concentrations, and describe the synthesis, single-crystal structures and solution data for charge-transfer complexes of the tridentate macrocycle [9]aneS_3 and the tetradentate macrocycles [12]-, [14]- and [16]-aneS_4.†

Results and Discussion

Solid-state studies

All compounds described were prepared by allowing a solution of the appropriate macrocycle and I_2 in CH_2Cl_2 to evaporate slowly. Crystals suitable for single-crystal X-ray diffraction studies deposited slowly, usually near the bottom of the reaction vessel, and were collected. The adduct 2[9]aneS_3·4I_2 **1** can be prepared either as described above by slow evaporation of a solution of I_2 and [9]aneS_3 in CH_2Cl_2 or by reaction of 2 molar equivalents of ICl with 1 molar equivalent of [9]aneS_3 in CH_2Cl_2.[8,9] The initial yellow precipitate [9]aneS_3·2ICl converts slowly over a few months *via* sublimation into red-

† [9]aneS_3 = 1,4,7-Trithiacyclononae, [12]aneS_4 = 1,4,7,10-tetrathiacyclododecane, [14]aneS_4 = 1,4,8,11-tetrathiacyclotetradecane and [16]aneS_4 = 1,5,9,13-tetrathiacyclohexadecane.

Table 1 Selected bond lengths (Å), angles (°) and torsion angles (°) with estimated standard deviations (e.s.d.s) in parentheses for 2[9]aneS$_3$·4I$_2$ **1**

I(14)–I(14′)	2.785(2)	I(24)–I(11)	2.754(2)
I(14)–S(14)	2.870(6)	I(24)–S(24)	3.054(6)
I(17)–I(17′)	2.816(2)	I(27′)–I(27)	2.799(2)
I(17)–S(17)	2.760(6)	I(27)–S(27)	2.862(6)
I(11)–S(11)	3.017(6)		
I(14′)–I(14)–S(14)	178.35(14)	I(11)–S(11)–C(12)	101.5(8)
I(14)–S(14)–C(13)	95.2(7)	I(11)–I(24)–S(24)	168.39(13)
I(14)–S(14)–C(15)	99.2(8)	I(24)–S(24)–C(23)	93.8(8)
I(17′)–I(17)–S(17)	174.86(14)	I(24)–S(24)–C(25)	99.0(8)
I(17)–S(17)–C(16)	94.0(7)	I(27′)–I(27)–S(27)	177.27(14)
I(17)–S(17)–C(18)	96.8(8)	I(27)–S(27)–C(26)	99.7(7)
I(24)–I(11)–S(11)	176.18(12)	I(27)–S(27)–C(28)	98.8(7)
I(11)–S(11)–C(19)	87.9(7)		

S(11)–C(12)–C(13)–S(14)	−86.7(18)
C(12)–C(13)–S(14)–C(15)	71.6(18)
C(13)–S(14)–C(15)–C(16)	−123.6(17)
S(14)–C(15)–C(16)–S(17)	60(2)
C(15)–C(16)–S(17)–C(18)	75.3(18)
C(16)–S(17)–C(18)–C(19)	−113.9(16)
S(17)–C(18)–C(19)–S(11)	77.4(18)
C(18)–C(19)–S(11)–C(12)	−97.5(17)
C(19)–S(11)–C(12) –C(13)	132.2(17)
S(21)–C(22)–C(23)–S(24)	55(2)
C(22)–C(23)–S(24)–C(25)	−132.2(17)
C(23)–S(24)–C(25)–C(26)	57.8(19)
S(24)–C(25)–C(26)–S(27)	56(2)
C(25)–C(26)–S(27)–C(28)	−132.9(16)
C(26)–S(27)–C(28)–C(29)	59.0(19)
S(27)–C(28)–C(29)–S(21)	55(2)
C(28)–C(29)–S(21)–C(22)	−131.9(18)
C(29)–S(21)–C(22)–C(23)	58(2)

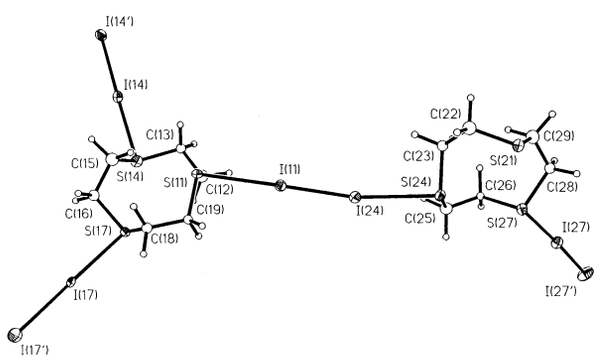

Fig. 1 Single-crystal structure of 2[9]aneS$_3$·4I$_2$ **1** with the numbering scheme adopted

brown crystals of composition 2[9]aneS$_3$·4I$_2$.[8] The single-crystal structures of the compounds obtained following those two routes are identical and show two independent [9]aneS$_3$ molecules which are bridged by an I$_2$ molecule [S(11)–I(11) 3.017(6), S(24)–I(24) 3.054(6) and I(11)–I(24) 2.754(2) Å; S(11)–I(11)–I(24) 176.18(12), S(24)–I(24)–I(11) 168.39(13)°] (Fig. 1, Table 1). One macrocycle is co-ordinated to another I$_2$ molecule [S(27)–I(27) 2.862(6), I(27)–I(27′) 2.799(2) Å; S(27)–I(27)–I(27′) 177.27(14)°] whereas the second macrocycle interacts with two I$_2$ molecules [S(14)–I(14) 2.870(6), I(14)–I(14′) 2.785(2), S(17)–I(17) 2.760(6) and I(17)–I(17′) 2.816(2) Å; S(14)–I(14)–I(14′) 178.35(14) and S(17)–I(17)–I(17′) 174.86(14)°]. The compound may therefore be regarded formally as an adduct between [9]aneS$_3$·I$_2$ and [9]aneS$_3$·3I$_2$[9] rather than being simply the dimer of [9]aneS$_3$·2I$_2$. However, the packing in **1** (Fig. 2) is complicated revealing extensive additional I···I and I···S contacts throughout the structure to give an extended network of interlinking macrocycles. One of the [9]aneS$_3$ molecules [S(21)–C(29)] adopts the same general

Table 2 Selected bond lengths (Å), angles (°) and torsion angles (°) with e.s.d.s in parentheses for [12]aneS$_4$·I$_2$ **2b** (I $1-x, -y, 2-z$; II $-x, -y, -z$)

I(21)–I(1)	2.7549(8)	I(7)–S(7)	3.203(2)
I(7)–I(7^{I})	2.7500(10)	I(21)–S(21)	3.148(2)
I(1)–S(1)	3.174(2)		
S(1)–I(1)–I(21)	174.99(4)	C(8′)–S(7)–I(7)	85.1(7)
C(12)–S(1)–I(1)	106.9(5)	C(6)–S(7)–I(7)	84.0(4)
C(2)–S(1)–I(1)	88.0(4)	S(21)–I(21)–I(1)	170.28(4)
S(7)–I(7)–I(7^{I})	165.00(4)	C(26^{II})–S(21)–I(21)	91.9(4)
C(8)–S(7)–I(7)	119.5(5)	C(22)–S(21)–I(21)	85.2(4)

C(2)–S(1)–C(12)–C(11)	−73.7(6)
C(12)–S(1)–C(2)–C(3)	−72.3(6)
S(1)–C(2)–C(3)–S(4)	173.2(4)
C(2)–C(3)–S(4)–C(5)	−76.0(6)
C(3)–S(4)–C(5)–C(6)	−76.3(6)
S(4)–C(5)–C(6)–S(7)	171.6(4)
C(5)–C(6)–S(7)–C(8)	−60.5(6)
C(6)–S(7)–C(8)–C(9)	−71.3(7)
S(7)–C(8)–C(9)–S(10)	173.9(5)
C(8)–C(9)–S(10)–C(11)	−81.0(7)
C(9)–S(10)–C(11)–C(12)	−64.4(7)
S(10)–C(11)–C(12)–S(1)	172.0(4)
S(21)–C(22)–C(23)–S(24)	172.0(4)
C(22)–C(23)–S(24)–C(25)	−79.3(6)
C(23)–S(24)–C(25)–C(26)	−82.3(6)
S(24)–C(25)–C(26)–S(21^{II})	167.0(4)
C(25)–C(26)–S(21^{II})–C(22^{II})	−90.7(6)
C(26)–S(21^{II})–C(22^{II})–C(23^{II})	94.8(6)

[333] conformation, which is found in the solid-state structure of free [9]aneS$_3$ with the S atoms adopting *exo* orientations.[15] However, the [9]aneS$_3$ moiety S(11)–C(19) adopts an unusual distorted [234] conformation. With a 1:3 molar ratio of [9]aneS$_3$:I$_2$, crystals of [9]aneS$_3$·3I$_2$, in which all the thioether donors are bound to I$_2$, can be obtained.[9] In this adduct the S–I [2.865(6)–2.933(4) Å] and I–I [2.772(1)–2.751(2) Å] distances are similar to those in 2[9]aneS$_3$·4I$_2$.

The single-crystal structure of [12]aneS$_4$·I$_2$ **2a** has been reported recently by Baker *et al.*[10] It consists of independent [12]aneS$_4$ molecules bridged symmetrically by I$_2$ molecules [S–I 3.220(3) and I–I 2.736(1) Å; S–I–I 170.5(1)°]. We were able to prepare[11] a similar compound with the same stoichiometry [12]aneS$_4$·I$_2$ **2b** but a different solid-state stucture. Compounds **2a** and **2b** both crystallise in the monoclinic crystal system ($P2_1/a$ and $P2_1/c$ respectively) but the unit-cell volume for **2b** (2190 Å^3) is approximately three times that for **2a** (740 Å^3). The asymmetric unit of **2b** therefore contains three times the number of atoms compared with **2a** (1.5 [12]aneS$_4$ and 1.5 I$_2$ molecules, Fig. 3). One macrocycle and one I$_2$ molecule lie on crystallographic inversion centres and the structure therefore contains a symmetric [S(7)–I(7) 3.203(2) and I(7)–I(7^{I}) 2.7500(10) Å; S(7)–I(7)–I(7^{I}) 165.00(4)°; I $1-x, -y, 2-z$] as well as an asymmetric [S(1)–I(1) 3.174(2), S(21)–I(21) 3.148(2) and I(1)–I(21) 2.7549(8) Å; S(1)–I(1)–I(21) 174.99(4) and S(21)–I(21)–I(1) 170.28(4)°] bridging I$_2$ moieties within the same structure (Table 2). The macrocycles in **2a** and S(21)–C(26) in **2b** adopt the typical [3333] conformation with *exo*-oriented S atoms which has also been found in the structure of free [12]aneS$_4$,[16] although the macrocycle S(1)–C(12) in **2b** adopts a distorted [2334] conformation. The alternating sequence of [12]aneS$_4$ and I$_2$ molecules results in infinite one-dimensional chains running in the [102] direction in the packing diagram (Fig. 4).

In [14]aneS$_4$·I$_2$ **3** (Fig. 5, Table 3) the macrocycle retains the [3434] conformation of free [14]aneS$_4$[17] and the I$_2$ molecules [I(1)–I(1′) 2.8095(11) Å; S(1)–I(1)–I(1′) 178.57(7)°] bridge asymmetrically between two independent [14]aneS$_4$ molecules [S(1)–I(1) 2.859(3) and S(8^{I})–I(1′) 3.640(3) Å; S(8^{I})–I(1′)–I(1) 168.38(5); I $-\frac{1}{2}+x, y, \frac{1}{2}-z$] thus forming an infinite one-

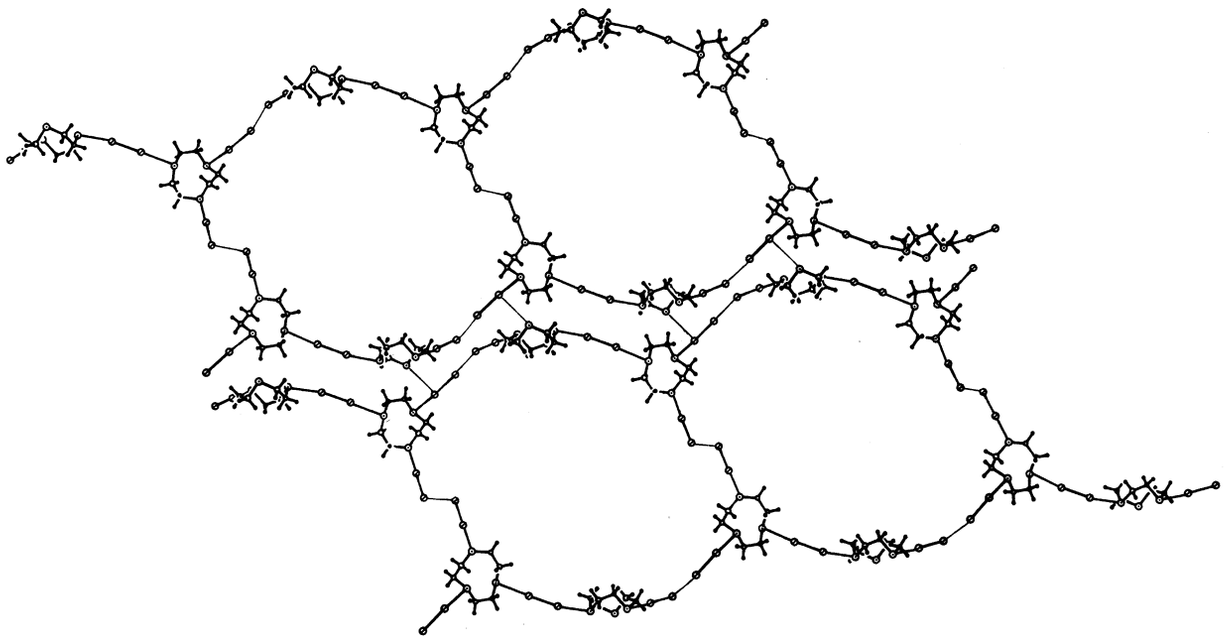

Fig. 2 Packing diagram of compound **1**

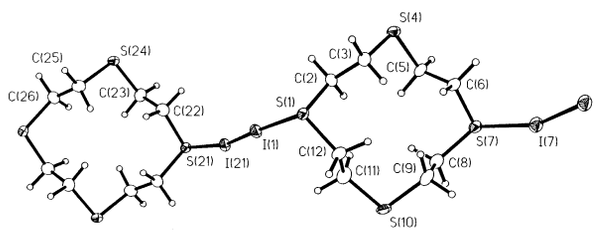

Fig. 3 Single-crystal structure of [12]aneS$_4$·I$_2$ **2b** with the numbering scheme adopted

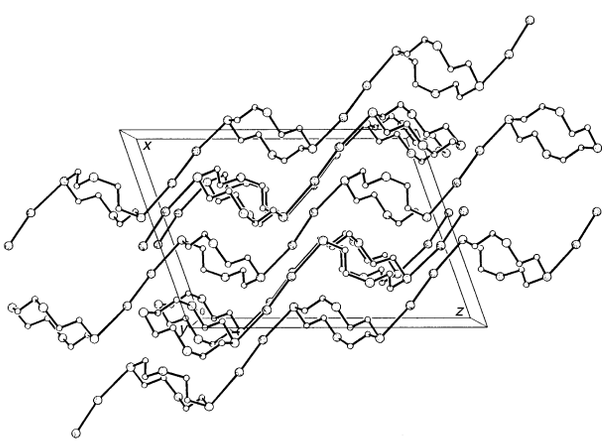

Fig. 4 Packing in [12]aneS$_4$·I$_2$ **2b** showing the infinite one-dimensional chain structure formed by alternating I$_2$ and [12]aneS$_4$ molecules

dimensional chain structure. However, the structure can also be visualised as having alternating layers of macrocycle and I_2 spanned by S · · · S contacts of 3.335(4) Å (Fig. 6).

The asymmetric unit of [14]aneS$_4$·2I$_2$ **4** comprises two independent half-macrocycles and two I_2 molecules (Fig. 7, Table 4). The S–I [S(11)–I(11) 2.800(4), S(21)–I(21) 2.841(4) Å] and I–I distances [I(11)–I(11′) 2.821(2), I(21)–I(21′) 2.808(2) Å] are very similar to those found for compound **3**. The S–I–I geometry is, as expected, essentially linear [S(11)–I(11)–I(11′) 177.58(8) and S(21)–I(21)–I(21′) 177.86(8)°]. Both macrocycles again adopt the [3434] conformation found in the solid-state structure of **3** and free [14]aneS$_4$.[17] The least-squares planes through the S atoms of the two macrocycles are tilted against

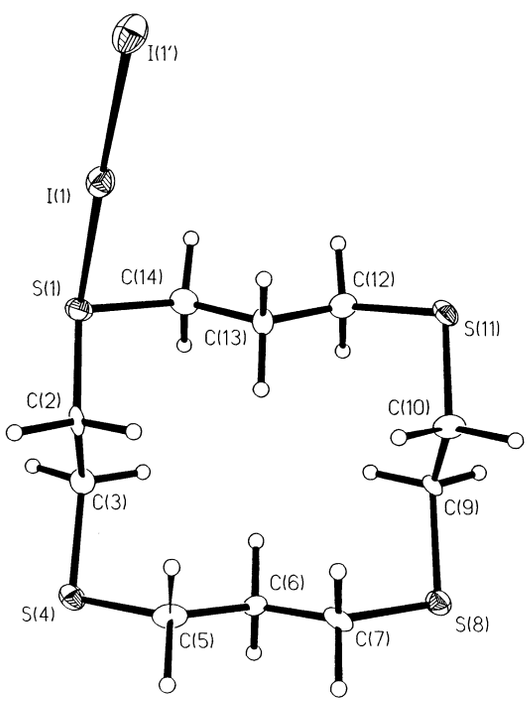

Fig. 5 Single-crystal structure of [14]aneS$_4$·I$_2$ **3** with the numbering scheme adopted

each other by about 47° leading to stacks of [14]aneS$_4$·2I$_2$ molecules in two different orientations in the packing diagram (Fig. 8). The presence of alternating sheets of macrocycle and I_2 is a feature also found in **3**. The arrangements within each stack are nevertheless very similar and this is reflected in the conformation of the macrocycles and the I–I and I–S distances. A view approximately along the *a* lattice direction showing the packing motif in **4** in which S · · · I interactions link molecules into a three-dimensional, infinite network is shown in Fig. 8. The network can be visualised as chains of molecules with alternating orientations running in the [011] direction and linked by S · · · I contacts of 3.699 Å (shown as thin dashed lines). These chains are cross-linked by longer S · · · I contacts of 3.931 Å (shown as dotted lines) to form layers. The I_2 centres involved in these contacts are derived exclusively from one of the two independent molecules and its symmetry equivalents.

Table 3 Selected bond lengths (Å), angles (°) and torsion angles (°) with e.s.d.s in parentheses for [14]aneS$_4$·I$_2$ **3** (I $-\frac{1}{2}+x, y, \frac{1}{2}-z$)

I(1)–I(1′)	2.8095(11)	I(1)–S(1)	2.859(3)
I(1′)–S(8^{I})	3.640(3)		
S(8^{I})–I(1′)–I(1)	168.38(5)	I(1)–S(1)–C(2)	108.3(4)
I(1′)–I(1)–S(1)	178.57(7)	I(1)–S(1)–C(14)	99.7(4)

S(1)–C(2)–C(3)–S(4)	−175.2(5)
C(2)–C(3)–S(4)–C(5)	−63.5(8)
C(3)–S(4)–C(5)–C(6)	−67.4(8)
S(4)–C(5)–C(6)–C(7)	177.8(7)
C(5)–C(6)–C(7)–S(8)	−176.8(7)
C(6)–C(7)–S(8)–C(9)	67.5(8)
C(7)–S(8)–C(9)–C(10)	69.7(8)
S(8)–C(9)–C(10)–S(11)	178.6(5)
C(9)–C(10)–S(11)–C(12)	54.5(9)
C(10)–S(11)–C(12)–C(13)	61.0(9)
S(11)–C(12)–C(13)–C(14)	172.4(7)
C(12)–C(13)–C(14)–S(1)	−175.6(7)
C(13)–C(14)–S(1)–C(2)	−55.0(9)
C(14)–S(1)–C(2)–C(3)	−64.8(8)

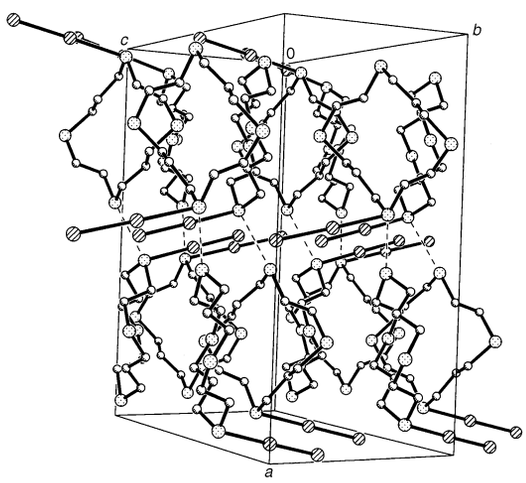

Fig. 6 Packing in [14]aneS$_4$·I$_2$ **3** showing alternating zones of macrocycle and I$_2$ along the *a* direction; S···S contacts link the macrocyclic layers across the I$_2$ sheets

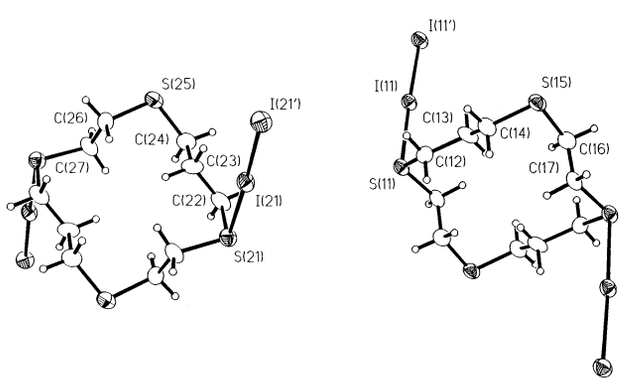

Fig. 7 Single-crystal structure of [14]aneS$_4$·2I$_2$ **4** with the numbering scheme adopted

Diiodine moieties from the other type of molecule participate in S···I contacts of 3.699 Å to molecules in layers above and below: these interactions are depicted as thick dashed lines in Fig. 8 and the three molecules representing an upper layer are identified by the letter A at their centre.

The 1:1 adduct [16]aneS$_4$·I$_2$ **5** exhibits features similar to those seen in **2a**, **2b** and **3**. Molecules of [16]aneS$_4$ lie on crystallographic inversion centres with a [233233] macrocyclic conformation (Fig. 9, Table 5) which is unexpectedly different

Table 4 Selected bond lengths (Å), angles (°) and torsion angles (°) with e.s.d.s in parentheses for [14]aneS$_4$·2I$_2$ **4** (I $-x, -y, 3-z$; II $-x, 1-y, 2-z$)

I(11)–I(11′)	2.821(2)	I(21)–I(21′)	2.808(2)
I(11)–S(11)	2.800(4)	I(21)–S(21)	2.841(4)
S(11)–I(11)–I(11′)	177.58(8)	S(21)–I(21)–I(21′)	177.86(8)
C(12)–S(11)–I(11)	104.9(5)	C(22)–S(21)–I(21)	101.2(4)
C(17^{I})–S(11)–I(11)	101.0(5)	C(27^{II})–S(21)–I(21)	101.1(5)

S(11)–C(12)–C(13)–C(14)	−177.2(10)
C(12)–C(13)–C(14)–S(15)	−178.5(9)
C(13)–C(14)–S(15)–C(16)	−61.8(12)
C(14)–S(15)–C(16)–C(17)	−67.5(10)
S(15)–C(16)–C(17)–S(11^{I})	−171.6(6)
C(16)–C(17)–S(11^{I})–C(12^{I})	−66.2(10)
C(17)–S(11^{I})–C(12^{I})–C(13^{I})	56.2(11)
S(21)–C(22)–C(23)–C(24)	−174.8(10)
C(22)–C(23)–C(24)–S(25)	−178.3(10)
C(23)–C(24)–S(25)–C(26)	−60.3(11)
C(24)–S(25)–C(26)–C(27)	−67.2(11)
S(25)–C(26)–C(27)–S(21^{II})	−167.5(7)
C(26)–C(27)–S(21^{II})–C(22^{II})	−66.6(11)
C(27)–S(21^{II})–C(22^{II})–C(23^{II})	54.5(11)

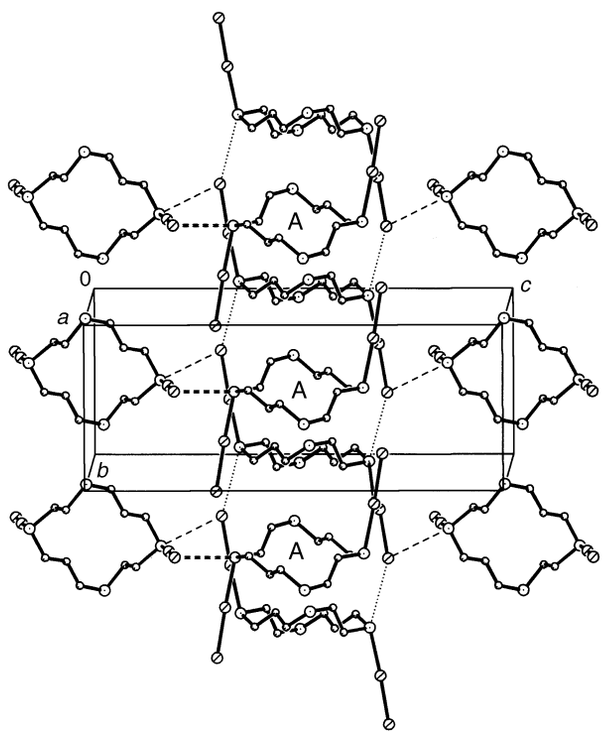

Fig. 8 Packing in [14]aneS$_4$·2I$_2$ **4** showing stacks in two distinct orientations within the crystal lattice

from the [3535] conformation of the uncomplexed macrocycle.[18] Nevertheless a common feature in both **5** and [16]aneS$_4$ is the presence of two *endo*-oriented S atoms, contrasting with the other tetradentate macrocycles [12]aneS$_4$ and [14]aneS$_4$. In **5** alternating [16]aneS$_4$ and I$_2$ molecules form infinite, one-dimensional chains running in the [111] direction as shown in Fig. 10. The I$_2$ bridges between independent macrocycles are symmetrical [I(1)–I(1^{I}) 2.773(12) and S(1)–I(1) 3.114(14) Å; S(1)–I(1)–I(1^{I}) 173.02(8)°; I = $-x, -y, -z$].

The compound [16]aneS$_4$·4I$_2$ **6** is the only example in the present investigation where all four S-donor atoms co-ordinate to I$_2$ molecules (Fig. 11, Table 6). The I(1)–I(1′) and I(5)–I(5′) distances of 2.8108(9) and 2.7916(8) Å and I(1)–S(1) and I(5)–S(5) distances of 2.756(2) and 2.848(2) Å are typical and very similar to those in **4**: the S–I–I moieties, as expected, are

Table 5 Selected bond lengths (Å), angles (°) and torsion angles (°) with e.s.d.s in parentheses for [16]aneS$_4$·I$_2$ **5** (I $-x$, $-y$, $-z$; II $1-x$, $1-y$, $1-z$)

I(1)–I(1^{I})	2.773(12)	S(1)–I(1)	3.114(14)
I(1^{I})–I(1)–S(1)	173.02(8)	I(1)–S(1)–C(8^{II})	92.6(5)
I(1)–S(1)–C(2)	92.9(6)		

S(1)–C(2)–C(3)–C(4)	−156.4(9)
C(2)–C(3)–C(4)–C(5)	74.7(13)
C(3)–C(4)–S(5)–C(6)	81.4(11)
C(4)–S(5)–C(6)–C(7)	−172.0(9)
S(5)–C(6)–C(7)–C(8)	82.7(12)
C(6)–C(7)–C(8)–S(1^{II})	173.6(9)
C(7)–C(8)–S(1^{II})–C(2^{II})	−165.1(9)
C(8)–S(1^{II})–C(2^{II})–C(3^{II})	78.6(10)

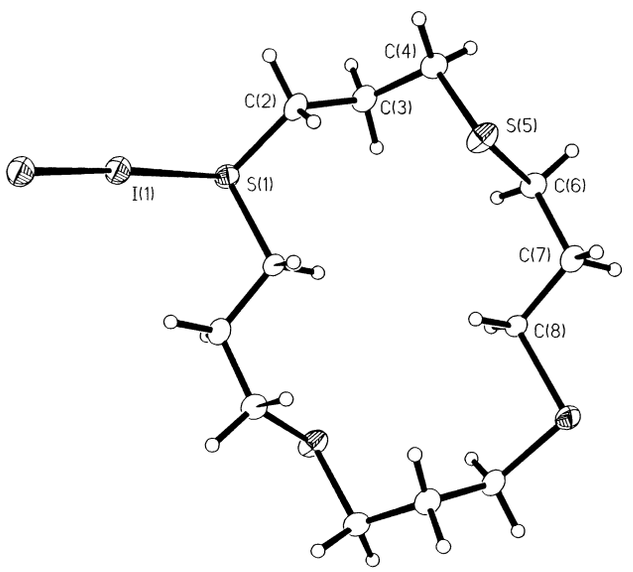

Fig. 9 Single-crystal structure of [16]aneS$_4$·I$_2$ **5** with the numbering scheme adopted

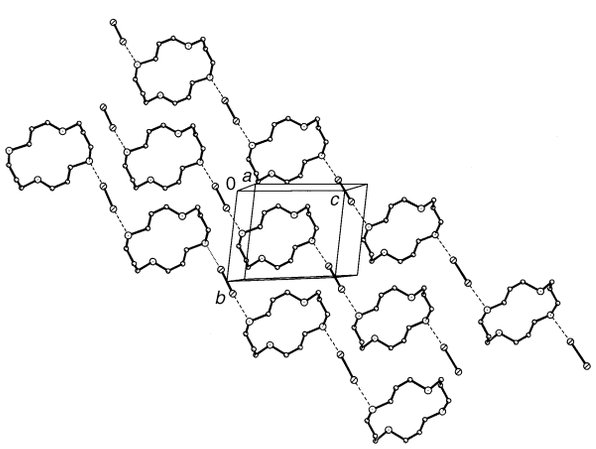

Fig. 10 Packing in [16]aneS$_4$·I$_2$ **5** which has a one-dimensional chain structure similar to that of compound **2b**

quasi-linear [S(1)–I(1)–I(1′) 174.74(5) and S(5)–I(5)–I(5′) 171.71(5)°]. Although the macrocycle lies on a crystallographic two-fold axis passing through C(15) and C(7) it adopts a [233233] conformation similar to that found in the structure of **5**, where the molecules lie on inversion centres. However, the conformations of the [16]aneS$_4$ macrocycle in **5** and **6** (Figs. 9 and 11, respectively) are different with respect to the orientation of the S atoms. The packing diagram of **6** reveals a stacked arrangement of the macrocycles embedded in a matrix of I$_2$. The most significant intermolecular interactions are I···I con-

Table 6 Selected bond lengths (Å), angles (°) and torsion angles (°) with e.s.d.s in parentheses for [16]aneS$_4$·4I$_2$ **6** (I $-x$, y, $\frac{1}{2}-z$)

I(1)–I(1′)	2.8108(9)	I(5)–I(5′)	2.7916(8)
I(1)–S(1)	2.756(2)	I(5)–S(5)	2.848(2)
I(1′)–I(1)–S(1)	174.74(5)	I(5′)–I(5)–S(5)	171.71(5)
I(1)–S(1)–C(16)	95.8(3)	I(5)–S(5)–C(4)	107.4(3)
I(1)–S(1)–C(2)	108.6(3)	I(5)–S(5)–C(6)	93.7(3)

C(16^{I})–C(15)–C(16)–S(1)	68.9(7)
C(15)–C(16)–S(1)–C(2)	−166.1(5)
C(16)–S(1)–C(2)–C(3)	73.3(6)
S(1)–C(2)–C(3)–C(4)	166.4(6)
C(2)–C(3)–C(4)–S(5)	−177.6(6)
C(3)–C(4)–S(5)–C(6)	81.8(7)
C(4)–S(5)–C(6)–C(7)	−162.5(6)
S(5)–C(6)–C(7)–C(6^{I})	76.1(7)

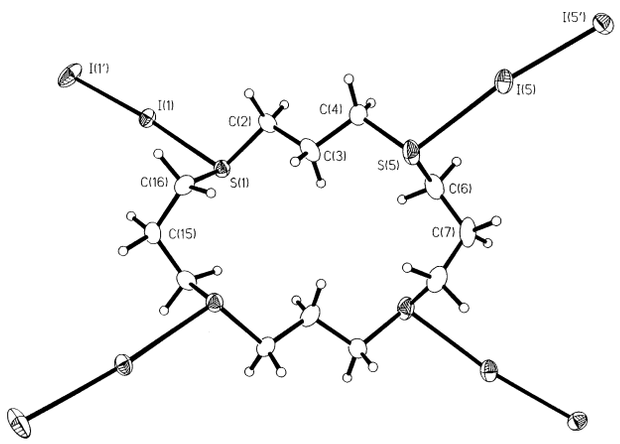

Fig. 11 Single-crystal structure of [16]aneS$_4$·4I$_2$ **6** with the numbering scheme adopted

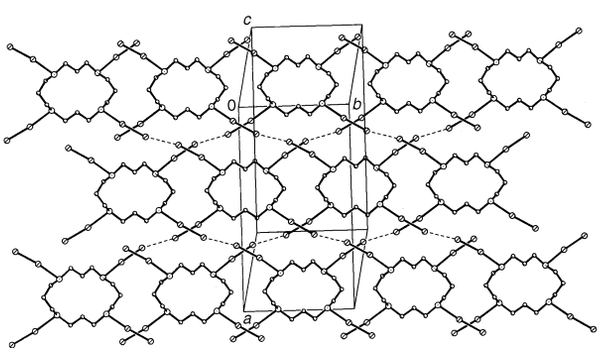

Fig. 12 Packing in [16]aneS$_4$·4I$_2$ **6**. Molecules are linked by I···I contacts into infinite chains which are interwoven to form a corrugated bilayer

tacts of 3.639(2) Å, which link molecules into two-dimensional, interwoven corrugated sheets lying in the *ab* plane (Fig. 12). Each molecule is linked to four of its neighbours *via* their terminal I$_2$ atoms: two of these neighbours lie in the upper part of the bilayer and two in the lower. Chains of molecules are nearly linear with I–I···I angles of 153.7(1) and 165.9(1)°. Any chain has its I$_2$···I$_2$ bridges consistently above or below those of the chains it crosses, and this relationship applies to each set of parallel chains (Fig. 12).

Fig. 13 shows a plot of S–I *vs.* I–I distances for solid-state structures of diiodine adducts of thioether crowns and related thioethers. It is clear that there is, as expected, a general inverse relationship between these distances, with S–I distances of greater than 3 Å being associated with bridging S···I$_2$···S fragments.

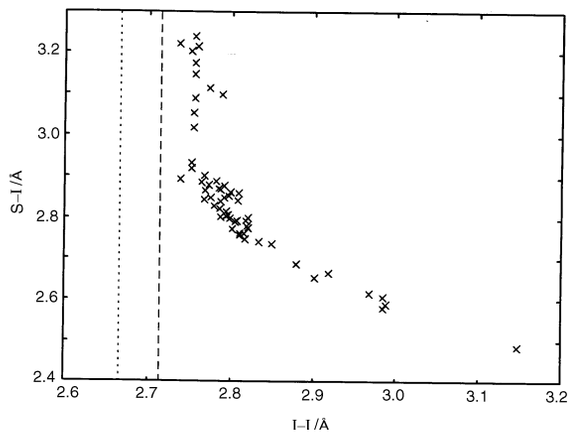

Fig. 13 Plot of S–I *vs.* I–I for structurally characterised adducts of thioethers and I_2. Dotted and dashed vertical lines denote the I–I distance in I_2 in the gas phase and solid state respectively

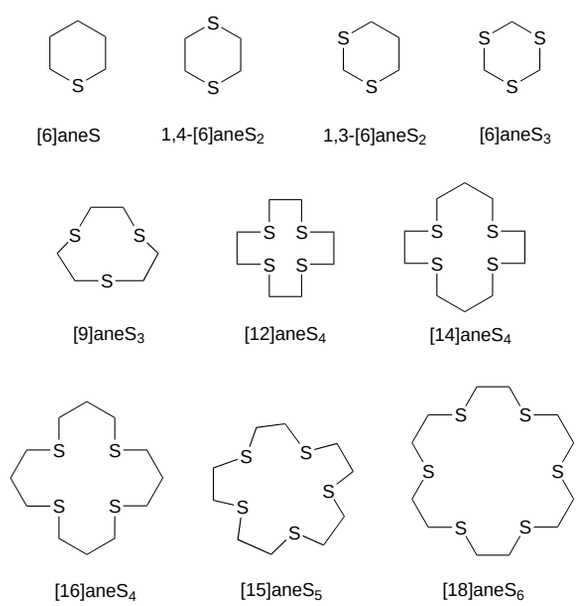

Solution studies

Electronic spectroscopic studies in solution allow measurement of the formation constants (K) and the thermodynamic parameters for the formation of charge-transfer adducts, equation (1).

$$D + I_2 \rightleftharpoons D{\cdot}I_2 \qquad (1)$$

Except for [6]aneS, all the thioether compounds under consideration contain two or more sulfur atoms capable of binding molecular I_2 and consequently molecular adducts having ligand:I_2 molar ratios different from 1:1 are to be expected in solution. Solutions containing both I_2 and suitable donors such as homoleptic thioether macrocycles in CH_2Cl_2 are dark brown in contrast to the violet colour of I_2 in CH_2Cl_2. The change from violet to brown ($\lambda_{max} = 490$ nm) upon addition of the thioether macrocycle indicates the formation of charge-transfer adducts in solution. It is important to establish the stoichiometry of the dissolved species and initially Job's method[19] of constant concentration variation was used to study the I_2–[9]aneS_3 system in CH_2Cl_2. The data (Table 7) strongly suggest that the predominant species under high dilution conditions has a 1:1 I_2:[9]aneS_3 composition. For all the macrocycles investigated, the electronic spectra of different solutions containing a constant amount of macrocycle and an increasing amount of I_2 up to a macrocycle:I_2 molar ratio of 1:5 were recorded. Only one isosbestic point was observed with each

Table 7 Absorbances at 308 ± 3 nm for 0.993 mmol dm^{-3} mixtures of diiodine and [9]aneS_3 in CH_2Cl_2

I_2:[9]aneS_3 ratio	Absorbance
0:10	0.000
1:9	0.056
2:8	0.097
3:7	0.129
4:6	0.150
5:5	0.164
6:4	0.142
7:3	0.130
8:2	0.103
9:1	0.070
10:0	0.000

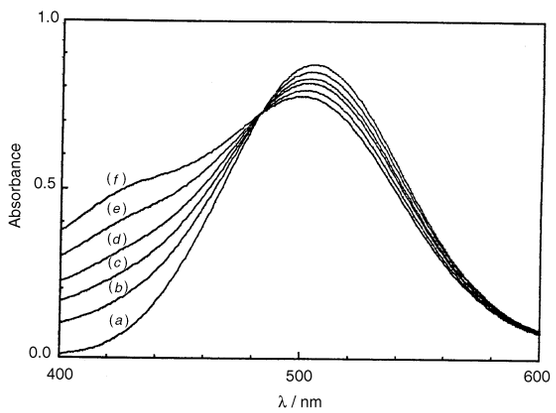

Fig. 14 Electronic spectra for addition of [18]aneS_6 to I_2. $[I_2] = 9.3 \times 10^{-4}$ mol dm^{-3} and $[[18]aneS_6] = 1.792 \times 10^{-4}$, 3.584×10^{-4}, 6.272×10^{-4}, 8.96×10^{-4}, 1.254×10^{-3} and 1.613×10^{-3} mol dm^{-3} for (*a*), (*b*), (*c*), (*d*), (*e*) and (*f*) respectively

macrocycle. Fig. 14 illustrates the isosbestic formation of the I_2 adduct of [18]aneS_6 up to a 1:5 [18]aneS_6:I_2 molar ratio. However, in order to avoid the formation of adducts different from 1:1, all the solutions used for the calculation of the stability constants of equilibrium (1) were prepared with macrocycle concentration always higher than that of I_2. Thus, under the conditions of the experimental spectrophotometric measurements, only the formation of the 1:1 adduct is relevant as confirmed by the presence of isosbestic points (Table 8) for all the compounds.

The formation constants K at 25 °C together with the ΔH values, calculated from plots of ln($K\varepsilon$) *versus* $1/T$, are reported in Table 9.‡[1] Values previously reported for [6]aneS_3 and [9]aneS_3 are also included.[9] The correlation coefficient ($r \geqslant 0.999$ for all compounds) for the plots of ln($K\varepsilon$) *versus* $1/T$ indicate a good reliability for the ΔH values. It should be emphasised that it has not always been possible to explore the whole range of the saturation fraction(s) with these substrates, which should spread from 0 to 1 for each set of solutions in order to have the best confidence in the calculated K and ε values.[21,22] In many cases either low solubility of the substrate or of the charge-transfer adduct prevented measurements throughout the full range of saturation fractions, s. For [6]aneS and [16]aneS_4 the accessible ranges of s were 0.11–0.95 and 0.21–0.91 (at 25 °C) respectively; for 1,4-[6]aneS_2, 1,3-[6]aneS_2, [14]aneS_4, [15]aneS_5 and [18]aneS_6 they were

‡ The molar absorption coefficients (ε) at six different wavelengths used for the calculation, the K values at temperatures of 15, 20, 25, 30 and 35 °C, the range of the saturation fraction experimentally realised for the sets of the solutions, the sum of the squared deviations between the calculated and observed absorbances, the ΔH values, calculated from the plots of ln($K\varepsilon$) *versus* $1/T$ and the correlation coefficients for the compounds are available from the authors.

Table 8 Charge-transfer band (λ_{CT}) molar absorption coefficients (ε_{CT}) and isosbestic points obtained between the I_2 visible band and its blue-shifted band (CH_2Cl_2 solutions, 25 °C) for thioether crowns

Compound	λ_{CT}/nm	ε_{CT}/dm^3 mol^{-1} cm^{-1}	Isosbestic point/nm
[6]aneS	305	27 300	474
1,4-[6]aneS$_2$	305	38 600	480
1,3-[6]aneS$_2$	310	26 500	480
[6]aneS$_3$	310	35 900	479
[9]aneS$_3$	310	26 200	480
[12]aneS$_4$	310	17 900	492
[14]aneS$_4$	310	30 900	482
[16]aneS$_4$	310	31 400	479
[15]aneS$_5$	310	25 800	490
[18]aneS$_6$	310	27 400	485

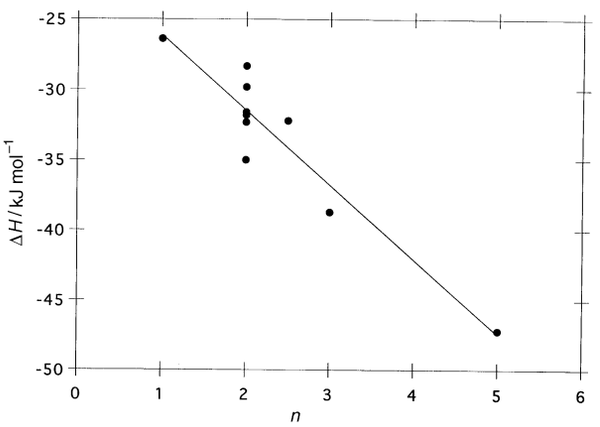

Fig. 15 Plot of ΔH *vs.* n (n = average number of CH_2 groups per sulfur atom) for I_2 adducts with thioether crowns

0.2–0.7, whereas those for [6]aneS$_3$, [9]aneS$_3$[9] and [12]aneS$_4$ were narrower at 0.05–0.25. Obviously, the narrower the range of *s* explored the less reliable are the values for *K*. For this reason, more reliable values of ΔH were obtained from plots of $\ln(K\varepsilon)$ *versus* $1/T$ in place of van't Hoff plots.§[,2]

Some preliminary conclusions can be drawn from inspection of the *K* values in Table 9. For rings of the same size the value of *K* decreases as the number of sulfur atoms increases. Otherwise, in the presence of the same number of sulfur atoms, *K* increases with increasing size of the ring (see for example the *K* values in Table 9 for the adducts of [6]aneS$_3$, [9]aneS$_3$ and [12]aneS$_4$, [14]aneS$_4$, [16]aneS$_4$). These trends can be explained in terms of inductive effects of the thioether atoms (−I) or *vice versa* in terms of the +I effect of the methylene groups. A convenient parameter that might take into account both these factors is the mean number of CH_2 groups (n) per sulfur atom. A rough correlation is found between the *K* values and n; compare for example the *K* value of [6]aneS$_3$ (13 dm^3 mol^{-1}, $n = 1$) with that of [9]aneS$_3$ (169 dm^3 mol^{-1}, $n = 2$) or the *K* values of [12]aneS$_4$ (74 dm^3 mol^{-1}), [14]aneS$_4$ (151 dm^3 mol^{-1}) and [16]aneS$_4$ (519 dm^3 mol^{-1}) for which $n = 2$, 2.5 and 3 respectively. However, since the values obtained for ΔH are more reliable than those for *K*, a plot of ΔH *vs.* n should be considered (Fig. 15). As can be seen, the values of ΔH do appear to depend upon n. However, all the compounds for which $n = 2$ show a high spread of ΔH values, indicating

§ As reported in the Experimental section, the formation constants *K* for the adduct of I_2 with 1,4-dithiacyclohexane were also calculated using SUPERSPEC.[20] The best values of *K* and ε obtained which minimise χ^2 are quite different from those reported in Table 9 [25 °C, $K = 104(18)$ dm^3 mol^{-1}]. However the value of ΔH obtained from a normal van't Hoff plot (31.8 ± 0.06 kJ mol^{-1}) is very similar to that in Table 9, thus supporting our choice of the method used in calculating ΔH.

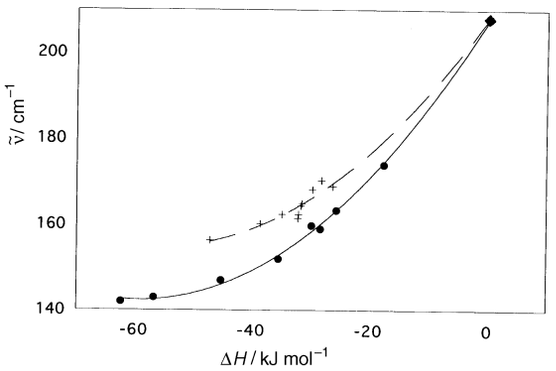

Fig. 16 Plot of ν(I–I) Raman *vs.* ΔH values. the lower curve (●) refers to diiodine–thioketone charge-transfer adducts, the upper (+) to the diiodine–thioether crown adducts. The value of 208 cm^{-1} ($\Delta H = 0$) (◆) refers to free I_2

that other factors such as solvation must inevitably affect the strength of the S–I_2 interaction. The existence of several potential conformers for each charge-transfer adduct in solution also appears likely, and may play an important role in the observed *K* and ΔH values. The presence of a range of possible conformers for these compounds is underlined clearly by X-ray studies on crystalline adducts with I_2 as described above.

In order to monitor further diiodine–thioether crown interactions, the Fourier-transform Raman spectra of CH_2Cl_2 solutions of a range of thioether crowns and I_2 have been recorded in the characteristic ν(I–I) region, and the Raman shifts and the band half-widths, $\Delta\nu_{\frac{1}{2}}$, are reported in Table 9. Although the band half-widths are affected by some uncertainty, they generally increase with the size of the ring, presumably reflecting an increased number of adduct conformers present in solution each with very slightly different I_2–S (thioether) bond strengths.

Fig. 16 shows a plot of the ν(I–I) Raman frequencies *vs.* ΔH values, together with data previously reported for the adducts obtained from compounds containing the C=S group.[23] The two sets of data do not fit the same curve and all the points corresponding to the thioether crowns lie above the curve obtained for the thioketones. This can be ascribed to the different hybridisation of the sulfur atoms in the two sets of compounds.

Conclusion

We have shown that diiodine charge-transfer adducts with homoleptic thioether macrocycles exhibit a range of different assemblies in the solid state and we have been able to identify and correlate those assemblies with the diiodine contents of the complex. Interestingly, regardless of ligand : I_2 ratios there is a tendency to obtain only certain adduct stoichiometries in the solid state. This reflects the solubility and packing behaviour of these isolated products. In particular, 1 : 1 adducts of I_2 and homoleptic S-donor macrocycles feature largely in this work and incorporate I_2-bridged chain structures. The overall conformation of these chains depends, however, very much on the conformational preferences of the macrocycles which accounts for instance for the differences in the structures of **2a**, **2b**, **3** and **5**. It is also interesting that the macrocycles in complexes with low diiodine content adopt similar conformations compared with the solid-state structure of the uncomplexed macrocycle.

In solution our findings strongly suggest that the 1 : 1 adduct is the predominant species. Electronic spectroscopy has been used to obtain formation constant data, and from the ΔH *vs.* ν(I–I) correlation it has been possible to evaluate the enthalpy of the S · · · I_2 donor–acceptor interaction.

A future paper will describe work on adducts of I_2 with penta-, hexa- and octa-dentate thioether macrocycles.

Table 9 Formation constants (K) at 25 °C, ΔH values, Raman frequencies ν(I–I) and their band half-width for adducts of I_2 with thioether crowns (standard deviations in parentheses)

Compound	n^a	K/dm^3 mol^{-1}	$-\Delta H$/kJ mol^{-1}	$\tilde{\nu}$(I–I)/cm^{-1}	$\Delta\nu_{\frac{1}{2}}$/cm^{-1}
[6]aneS	5	827(26)	47.2(0.1)	156	17
1,4-[6]aneS$_2$	2	40(1)	31.8(0.1)	164	19
1,3-[6]aneS$_2$	2	94(3)	32.3(0.3)	162	20
[6]aneS$_3$	1	13(1)	26.4(0.1)	169	21
[9]aneS$_3$	2	169(4)	35.0(0.1)	162	22
[12]aneS$_4$	2	74(7)	28.3(0.2)	170	*b*
[14]aneS$_4$	2.5	151(4)	32.2(0.1)	162	21
[16]aneS$_4$	3	519(9)	38.7(0.1)	160	19
[15]aneS$_5$	2	94(1)	29.8(0.1)	168	22
[18]aneS$_6$	2	151(2)	31.6(0.1)	165	23

[a] Number of methylene groups per sulfur atom. [b] Not reported since the low solubility of the adduct prevented the same precision as that for the other compounds.

Experimental

Spectrophotometric measurements were carried out using a Perkin-Elmer Lambda 9 UV/VIS/NIR spectrophotometer. Diiodine was purified by sublimation from KI and stored in a desiccator. A typical preparation consisted of mixing solutions of I_2 and the appropriate macrocycle in HPLC-grade CH_2Cl_2 affording about 15 cm^3 of a dark brown mixture. Slow evaporation at room temperature over a few weeks afforded products on the glass walls and the bottom of the reaction vessel. The products appeared in bands which could be distinguished by colour and morphology. It should be noted that most of these deposits were thin films covering the glass walls. Crystalline material suitable for single-crystal X-ray diffraction studies could in general only be recovered from near the bottom of the reaction vessel. The crystallisation products were collected and initially characterised by microanalysis. Larger deviations between observed and calculated values are commonly found for compounds with high diiodine contents, where loss of I_2 was apparent (Found: C, 11.25; H, 1.8. Calc. for $C_{12}H_{24}I_8S_6$ **1**: C, 10.5; H, 1.75. Found: C, 19.4; H, 3.3. Calc. for $C_8H_{16}I_2S_4$ **2b**: C, 19.45; H, 3.25. Found: C, 23.0; H, 3.95. Calc. for $C_{10}H_{20}I_2S_4$ **3**: C, 23.0; H, 3.85. Found: C, 13.05; H, 2.2. Calc. for $C_{12}H_{20}I_8S_4$ **6**: C, 11.0; H, 1.85%).

The relatively weak nature of the charge-transfer interaction in these compounds is reflected in mass spectral measurements which do not show molecular ion peaks for the adducts themselves but peaks assigned to I_2 and free macrocycle.

Crystallography

The following procedure is typical. A single crystal suitable for X-ray diffraction studies was mounted in the cold dinitrogen stream of an Oxford Cryosystems low-temperature device[24] on a Stoë Stadi-4 four-circle diffractometer [graphite-monochromated Mo-Kα X-radiation (λ = 0.710 73 Å); data acquisition by ω–2θ scan mode]. Other details of crystal data, data collection and processing and structure analysis are given in Table 10. The single-crystal structures of compounds **1**, **2b** and **6** were solved by direct methods using SHELXS 86.[25] A Patterson synthesis revealed the positions of the I atoms in the structures of **4** and **5** using SHELXS 86[25] and in **3** using SHELX 76.[26] The structures were developed by iterative cycles of least-squares refinement and ΔF synthesis. Excessive residual electron density in close proximity to I atoms at isotropic convergence warranted a further empirical absorption correction (DIFABS[27]) in the case of compounds **1**, **3** and **5**. All non-hydrogen atoms were refined anisotropically, except in the structure of **2b** where the minor components of the C atom disorder were allowed only thermal isotropic motion. Hydrogen atoms were included in calculated positions riding on the parent C atom. Their thermal parameters were either refined to a common U_{eq} (0.0236, 0.0312, 0.0342 and 0.0497 Å^2 in compounds **1**, **2b**, **3** and **6** respectively) or assigned 1.2 times the isotropic U_{eq} value of the parent C atom (in **4** and **5**). In Figs. 1, 3, 5, 7, 9 and 11 displacement ellipsoids are drawn at the 50% probability level and H atoms are represented by small spheres of arbitrary radii. Illustrations were generated using SHELXTL-PC,[28] and molecular geometry calculations utilised CALC,[29] SHELXTL-PC and SHELXL 93.[30]

The S(7)C(8)C(9)S(10) region in [12]aneS$_4$·I$_2$ **2b** was affected by disorder which was successfully modelled by allowing alternative positions for C(8) and C(9) with site occupancy factors of 0.75 and 0.25. All C–C and C–S distances in this region were restrained to 1.52 and 1.82 Å respectively and the minor components C(8′) and C(9′) were refined isotropically.

Atomic coordinates, thermal parameters, and bond lengths and angles have been deposited at the Cambridge Crystallographic Data Centre (CCDC). See Instructions for Authors, *J. Chem. Soc.*, *Dalton Trans.*, 1997, Issue 1. Any request to the CCDC for this material should quote the full literature citation and the reference number 186/325.

Solution studies

Two solutions of I_2 (0.993 mmol dm^{-3}) and [9]aneS$_3$ (0.993 mmol dm^{-3}) in CH_2Cl_2 were made up and the absorbance of 11 mixtures ranging from 0:10 to 10:0 ratio were measured at λ_{max} = 308 ± 3 nm in 0.3 mm cuvettes using a Perkin-Elmer Lambda 9 spectrophotometer. A plot of the measured absorbances against the I_2:[9]aneS$_3$ ratio gave a curve with a maximum of 0.98:1.02 I_2:[9]aneS$_3$ determined by the intersection of two linear regression tangents on either side of the curve. The 11 spectra recorded showed an isosbestic point at 480 nm.

Spectrophotometric measurements and data treatment. The spectrophotometric measurements for the determination of formation constants were carried out in CH_2Cl_2 solutions by using a Varian Cary 5 spectrophotometer having a temperature-controller accessory and connected to an IBM PS2 computer. The spectra of 12 different solutions were recorded in the range 250–600 nm at temperatures 15, 20, 25, 30 and 35 °C. The concentrations of the reagents were chosen according to criteria outlined in ref. 31 and discussed in previous papers.[21,22] In all the solutions the macrocycle concentrations were always higher than that of I_2 in order to avoid or at least minimise the formation of higher adducts. The sets of data for all thioether–diiodine solutions were analysed using a factor-analysis program[32] to determine the number of species present in solution. In all cases the presence of only two species, namely I_2 and the 1:1 L:I_2 adduct, has been confirmed. Data analysis was carried out with a program based on a non-linear least-squares method,[33] assuming that the best values of K and ε are those which minimise the sum of the function $\chi^2 = \Sigma (A_c - A_s)^2/(N - 2)$, where A_c and A_s are the calculated and experimental absorbances and N is the number of data points. The optimis-

Table 10 Experimental data for single-crystal structure determinations of 2[9]aneS$_3$·4I$_2$ **1**, [12]aneS$_4$·I$_2$ **2b**, [14]aneS$_4$·I$_2$ **3**, [14]aneS$_4$·2I$_2$ **4**, [16]aneS$_4$·I$_2$ **5** and [16]aneS$_4$·4I$_2$ **6**

Compound	**1**	**2b**	**3**	**4**	**5**	**6**
Formula	$C_{12}H_{24}I_8S_6$	$C_8H_{16}I_2S_4$	$C_{10}H_{20}I_2S_4$	$C_{10}H_{20}I_4S_4$	$C_{12}H_{24}I_2S_4$	$C_{12}H_{24}I_8S_4$
M	1375.88	494.25	522.31	776.10	550.39	1311.76
Crystal size/mm	0.70 × 0.08 × 0.04	0.35 × 0.33 × 0.12	0.30 × 0.25 × 0.05	0.62 × 0.62 × 0.54	0.31 × 0.15 × 0.04	0.25 × 0.20 × 0.10
Crystal system	Triclinic	Monoclinic	Orthorhombic	Monoclinic	Triclinic	Monoclinic
Space group	$P\bar{1}$ (no. 2)	$P2_1/c$ (no. 14)	*Pbca* (no. 61)	$P2_1/a$ (alt.$P2_1/c$ no. 14)	$P\bar{1}$ (no. 2)	$C2/c$ (no. 15)
a/Å	8.437(7)	13.882(4)	19.445(2)	9.362(3)	5.420(14)	21.236(8)
b/Å	13.82(2)	8.550(3)	17.509(2)	9.295(3)	8.05(4)	11.693(6)
c/Å	14.752(10)	19.563(6)	9.7030(11)	23.016(9)	10.74(3)	14.771(6)
α/°	65.95(5)				97.4(3)	
β/°	89.31(4)	109.44(3)		92.38(7)	95.1(2)	123.710 (14)
γ/°	81.08(4)				94.9(3)	
U/Å^3	1549	2190	3304	2001	461	3051
Z	2	6	8	4	1	4
D_c/g cm^{-3}	2.949	2.249	2.100	2.576	1.984	2.855
μ/mm^{-1}	8.32	4.78	4.23	6.63	3.80	8.32
F(000)	1232	1404	2000	1424	266	2336
$2\theta_{max}$/°	40	45	45	50	45	45
hkl Ranges	−8 to 8, −11 to 13, 0–14	−14 to 14, 0–9, 0–21	0–20, 0–18, 0–10	−11 to 11, 0–11, 0–27	−5 to 5, −8 to 8, 0–11	−22 to 15, −12 to 0, −15 to 15
Measured reflections	2897	3097	3200	3695	1204	2105
Independent reflections, R_{int}	2897,—	2743,—	1930, 0.014	3443, 0.0654	1204,—	1827,—
Observed reflections	2405 [$F \geqslant 4\sigma(F)$]	2589 [$F \geqslant 4\sigma(F)$]	1462 [$F \geqslant 4\sigma(F)$]	3370 [$F \geqslant 2\sigma(F)$]	1053 [$F \geqslant 2\sigma(F)$]	1712 [$F \geqslant 4\sigma(F)$]
Maximum, minimum ψ-scan correction	0.891, 0.269	0.411, 0.238	0.398, 0.198	0.023, 0.007	0.337, 0.219	0.906, 0.557
Full-matrix least squares on	F	F	F	F^2	F^2	F
using	SHELX 76	SHELX 76	SHELX 76	SHELXL 93	SHELXL 93	SHELX 76
Maximum, minimum DIFABS correction	1.390, 0.643	—	1.245, 0.811	—	1.236, 0.667	—
Parameters refined	177	201	147	163	82	112
SHELX 76[a] R, R', S	0.057, 0.073, 0.85	0.037, 0.056, 1.01	0.037, 0.041, 0.99	—	—	0.027, 0.032, 1.12
x	0.000 961	0.000 363	0.000 206			0.000 48
SHELXL 93[b] $R1$, $wR2$, S	—	—	—	0.077, 0.212, 1.11	0.073, 0.199, 1.09	—
A, B	—	—	—	0.085, 43.89	0.1647, 1.14	—
$(\Delta/\sigma)_{max}$	0.001	0.001	0.032	0.000	0.051	0.001
$\Delta\rho_{max,\ min}$/e Å^{-3}	+2.23, −1.86	+1.24, −1.37	+0.84, −0.77	+2.20, −1.93	+2.93, −1.96	+1.63, −1.30

[a] Weighting scheme $w^{-1} = \sigma^2(F) + xF^2$, S (goodness of fit) = $[\Sigma w(|F_o| - |F_c|)^2/(N_o - N_p)]^{\frac{1}{2}}$. [b] Weighting scheme $w^{-1} = [\sigma^2(F_o^2) + (AP)^2 + BP]$ where $P = [\max(F_o^2, 0) + 2F_c^2]/3$, $S = [\Sigma w(F_o^2 - F_c^2)^2]/(n - p)]^{\frac{1}{2}}$.

ation of K was carried out at six different wavelengths. For some compounds the calculated K and ε values were correlated with an observed decrease in ε with increase in temperature. The value of ΔH were therefore calculated by averaging the slopes of the six straight lines obtained by plotting $\ln(K\varepsilon)$ *versus* $1/T$ at six different wavelengths; $\Delta H = (\Sigma \Delta H_i/\sigma_i)/\Sigma 1/\sigma_i$, $\sigma = \{(N-1)\Sigma\sigma_i^2/[Nn(Nn-1)]\}^{\frac{1}{2}}$, where N and n are the numbers of the different temperatures and wavelengths respectively. This procedure provides more reliable values of ΔH than those obtainable by using a van't Hoff plot. In addition to the factor analysis,[32] a new set of electronic spectra for 1,4-dithiacyclohexane were recorded. Fifteen solutions having a constant concentration of 1,4-dithiacyclohexane (3.999×10^{-3} mol dm^{-3}) and increasing amounts of I_2 (I_2: donor molar ratio ranging from 0.1 to 30:1) were analysed with the SUPERSPEC program,[20] giving convergence of unique values for K and ε confirming the formation of the 1:1 adduct only.

Fourier-transform Raman spectra. The Fourier-transform Raman spectra were recorded on an FRA 106 FT Raman accessory mounted on a Bruker IFS 66 FT-IR vacuum instrument, operating with an excitation frequency of 1064 nm (Nd−YAG laser). No sample decomposition was observed during the experiments. The solutions used contained 0.8:1.0 molar ratios of diiodine:macrocycle, $[I_2] = 2.6 \times 10^{-2}$ mol dm^{-3}.

Acknowledgements

We thank the EPSRC for support and the Comitato Nazionale per le Scienze Chimiche of Consiglio Nazionale delle Ricerche (Rome) for financial support.

References

1 O. Hassel and G. Eia, *Acta Chem. Scand.*, 1956, **10**, 139; K. O. Strømme, *Acta Chem. Scand.*, 1959, **13**, 268; O. Hassel and H. Hope, *Acta Chem. Scand.*, 1960, **14**, 391; O. Hassel, O. Rømming and T. Tufte, *Acta Chem. Scand.*, 1961, **15**, 967; O. Hassel and C. Rømming, *Acta Chem. Scand.*, 1956, **10**, 696; T. Uchida, *Bull. Chem. Soc. Jpn.*, 1967, **40**, 2244; T. Uchida and K. Kimura, *Acta Crystallogr., Sect. C*, 1984, **40**, 139.
2 W. W. Schweikert and E. A. Meyers, *J. Phys. Chem.*, 1968, **72**, 1561; J. W. Bransford and E. A. Meyers, *Cryst. Struct. Commun.*, 1978, **7**, 697; F. A. Cotton and P. A. Kibala, *J. Am. Chem. Soc.*, 1987, **109**, 3308; N. Bricklebank, S. M. Godfrey, A. G. Mackie, C. A. McAuliffe and R. G. Pritchard, *J. Chem. Soc., Chem. Commun.*, 1992, 355.
3 O. Hassel and J. Hvoslef, *Acta Chem. Scand.*, 1956, **10**, 138.
4 F. H. Herbstein and W. Schwotzer, *J. Am. Chem. Soc.*, 1984, **106**, 2367; E. L. Ahlsen and K. O. Strømme, *Acta Chem. Scand., Ser. A*, 1974, **28**, 175.
5 F. Cristiani, F. Demartin, F. A. Devillanova, F. Isaia, G. Saba and G. Verani, *J. Chem. Soc., Dalton Trans.*, 1992, 3553.
6 C. Rømming, *Acta Chem. Scand.*, 1960, **14**, 2145; G. Allegra, G. E. Wilson, jun., E. Benedetti, C. Pedone and R. Albert, *J. Am. Chem. Soc.*, 1970, **92**, 4002; A. L. Tipton, M. C. Lonergan, C. L. Stern and D. F. Shriver, *Inorg. Chim. Acta*, 1992, **201**, 23.
7 J. D. McCullough, G. Y. Chao and D. E. Zuccaro, *Acta Crystallogr.*, 1959, **12**, 815.
8 A. J. Blake, R. O. Gould, C. Radek and M. Schröder, *J. Chem. Soc., Chem. Commun.*, 1993, 1191.
9 F. Cristiani, F. A. Devillanova, F. Isaia, V. Lippolis, G. Verani and F. Demartin, *Heteroatom. Chem.*, 1993, **4**, 571.
10 P. K. Baker, S. D. Harris, M. C. Durrant, D. L. Hughes and R. L. Richards, *Acta Crystallogr., Sect. C*, 1995, **51**, 697.
11 F. Cristiani, F. A. Devillanova, A. Garau, F. Isaia, V. Lippolis, G. Verani, F. Demartin, A. J. Blake, R. O. Gould, C. Radek and M. Schröder, *Synth. Methodologies Inorg. Chem.*, 1994, **4**, 406.
12 H. Hope and J. D. McCullough, *Acta Crystallogr.*, 1964, **17**, 712; H. Maddox and J. D. McCullough, *Inorg. Chem.*, 1966, **5**, 522; C. Knobler and J. D. McCullough, *Inorg. Chem.*, 1968, **7**, 365; G. Y. Chao and J. D. McCullough, *Acta Crystallogr.*, 1961, **14**, 940.
13 F. van Bolhuis, P. B. Koster and T. Migchelsen, *Acta Crystallogr.*, 1967, **23**, 940.
14 I. L. Karle, *J. Chem. Phys.*, 1955, **23**, 1739.
15 R. S. Glass, G. S. Wilson and W. N. Setzer, *J. Am. Chem. Soc.*, 1980, **102**, 5068; R. Blom, D. W. H. Rankin, H. E. Robertson, M. Schröder and A. Taylor, *J. Chem. Soc., Perkin Trans. 2*, 1991, 773.
16 R. E. Wolf, jun., J. R. Hartman, J. M. E. Storey, B. M. Foxman and S. R. Cooper, *J. Am. Chem. Soc.*, 1987, **109**, 4328; G. H. Robinson and S. A. Sangokoya, *J. Am. Chem. Soc.*, 1988, **110**, 1494.
17 R. E. DeSimone and M. D. Glick, *J. Am. Chem. Soc.*, 1976, **98**, 762.
18 A. J. Blake, R. O. Gould, M. A. Halcrow and M. Schröder, *Acta Crystallogr., Sect. B*, 1993, **49**, 773.
19 P. Job, *Anal. Chim.*, 1928, **9**, 113; 1936, **17**, 97.
20 F. Bigoli, P. Deplano, M. L. Mercuri, M. A. Pellinghelli, A. Sabatini, E. F. Trogu and A. Vacca, *Can. J. Chem.*, 1995, **73**, 380.
21 G. Carta, G. Crisponi and V. Nurchi, *Tetrahedron*, 1981, **37**, 2115.
22 G. Carta and G. Crisponi, *J. Chem. Soc., Perkin Trans. 2*, 1982, 53.
23 F. Cristiani, F. A. Devillanova, A. Garau, F. Isaia, V. Lippolis and G. Verani, *Heteroatom. Chem.*, 1994, **5**, 421.
24 J. Cosier and A. M. Glazer, *J. Appl. Crystallogr.*, 1986, **19**, 105.
25 G. M. Sheldrick, SHELXS 86, *Acta Crystallogr., Sect. A*, 1990, **46**, 467.
26 G. M. Sheldrick, SHELX 76, University of Cambridge, 1976.
27 N. Walker and D. Stuart, DIFABS, program for applying empirical absorption corrections, *Acta Crystallogr., Sect. A*, 1983, **39**, 158.
28 G. M. Sheldrick, SHELXTL-PC, Siemens Analytical X-Ray Instrumentation Inc., Madison, WI, 1994.
29 R. O. Gould and P. Taylor, CALC, program for molecular geometry calculations. The University of Edinburgh, 1985.
30 G. M. Sheldrick, SHELXL 93, University of Göttingen, 1993.
31 F. A. Devillanova and G. Verani, *Tetrahedron*, 1979, **35**, 511.
32 H. Gampp, M. Maeder, C. J. Meyer and A. Zuberbühler, *Talanta*, 1985, **32**, 95.
33 G. Crisponi and V. Nurchi, *J. Chem. Educ.*, 1989, **66**, 54.

Received 5*th August* 1996; *Paper* 6/05476E